



Donald A. Morgan,¹ Latisha N. McDaniel,² Terry Yin,² Michael Khan,²
Jingwei Jiang,¹ Michael R. Acevedo,³ Susan A. Walsh,³ Laura L. Boles Ponto,^{4,5}
Andrew W. Norris,⁵ Michael Lutter,^{2,6,7} Kamal Rahmouni,^{1,6,7} and Huxing Cui^{1,2,6}



Regulation of Glucose Tolerance and Sympathetic Activity by MC4R Signaling in the Lateral Hypothalamus

Diabetes 2015;64:1976–1987 | DOI: 10.2337/db14-1257

Melanocortin 4 receptor (MC4R) signaling mediates diverse physiological functions, including energy balance, glucose homeostasis, and autonomic activity. Although the lateral hypothalamic area (LHA) is known to express MC4Rs and to receive input from leptin-responsive arcuate proopiomelanocortin neurons, the physiological functions of MC4Rs in the LHA are incompletely understood. We report that MC4R^{LHA} signaling regulates glucose tolerance and sympathetic nerve activity. Restoring expression of MC4Rs specifically in the LHA improves glucose intolerance in obese MC4R-null mice without affecting body weight or circulating insulin levels. Fluorodeoxyglucose-mediated tracing of whole-body glucose uptake identifies the interscapular brown adipose tissue (iBAT) as a primary source where glucose uptake is increased in MC4R^{LHA} mice. Direct multifiber sympathetic nerve recording further reveals that sympathetic traffic to iBAT is significantly increased in MC4R^{LHA} mice, which accompanies a significant elevation of Glut4 expression in iBAT. Finally, bilateral iBAT denervation prevents the gluco-regulatory effect of MC4R^{LHA} signaling. These results identify a novel role for MC4R^{LHA} signaling in the control of sympathetic nerve activity and glucose tolerance independent of energy balance.

The incidence and prevalence of obesity and associated disorders, such as diabetes and hypertension, are increasing

worldwide (1). Although there is a general consensus that the central nervous system (CNS) plays a key role in these processes (2,3), the underlying neural substrates remain to be fully defined. The central melanocortin signaling pathway, mainly through action on the melanocortin 4 receptors (MC4Rs), is a key relay of arcuate proopiomelanocortin and agouti-related peptide-expressing neurons to coordinate long-term energy balance, glucose homeostasis, and sympathetic nerve activity (SNA) (4). Loss of function of MC4R in both humans and rodents leads to the development of obesity, insulin resistance, and diabetes (5,6). MC4Rs are widely expressed in the CNS, including certain hypothalamic nuclei implicated in the regulation of energy balance, glucose metabolism, and sympathetic outflow, including the paraventricular nucleus, dorsomedial nucleus, and lateral hypothalamic area (LHA) (7). Previous studies identified distinct roles of MC4R signaling in specific neural circuits (8–11), offering the possibility that discrete functions of MC4R signaling in specific CNS sites will allow the development of selective treatments for obesity and associated disorders. The LHA, which receives direct input from leptin-responsive arcuate proopiomelanocortin neurons (12) and expresses MC4Rs (7), regulates multiple physiological processes, including food intake, reward-related behaviors, and autonomic function (13,14). However, the physiological role of MC4R signaling in the LHA is incompletely understood. We have previously shown that MC4R^{LHA} neurons coexpress

¹Department of Pharmacology, University of Iowa, Carver College of Medicine, Iowa City, IA

²Department of Psychiatry, University of Iowa, Carver College of Medicine, Iowa City, IA

³Small Animal Imaging Core, University of Iowa, Carver College of Medicine, Iowa City, IA

⁴Department of Radiology, University of Iowa, Carver College of Medicine, Iowa City, IA

⁵Department of Pediatrics, University of Iowa, Carver College of Medicine, Iowa City, IA

⁶Fraternal Order of Eagles Diabetes Research Center, University of Iowa, Carver College of Medicine, Iowa City, IA

⁷Obesity Research and Education Initiative, University of Iowa, Carver College of Medicine, Iowa City, IA

Corresponding author: Huxing Cui, huxing-cui@uiowa.edu.

Received 15 August 2014 and accepted 10 January 2015.

This article contains Supplementary Data online at <http://diabetes.diabetesjournals.org/lookup/suppl/doi:10.2337/db14-1257/-/DC1>.

© 2015 by the American Diabetes Association. Readers may use this article as long as the work is properly cited, the use is educational and not for profit, and the work is not altered.

the anorectic peptide neurotensin and functionally active form of the leptin receptor and are responsive to leptin administration (15). These observations suggested a potential role for MC4R^{LHA} neurons in metabolic regulation. Using a Cre-dependent reactivatable MC4R-null mouse line (8), we investigated the physiological function of MC4R^{LHA} signaling, with a specific focus on energy balance, glucose metabolism, and autonomic activity.

RESEARCH DESIGN AND METHODS

Animals

Mice with a transcriptional blocking (TB) cassette flanked by loxP sites placed in front of the MC4R gene (MC4R-TB) and backcrossed at least six generations onto the C57BL/6 line were previously reported (8,16). The tdTomato reporter mice were purchased from The Jackson Laboratory (stock number 007909). Mice were housed in the University of Iowa vivarium in a temperature-controlled environment (lights on 0600–1800 h) with ad libitum access to water and food. To avoid the potentially confounding effects of the female estrus cycle on metabolic profiling, only male mice were used. All animal procedures were performed in accordance with University of Iowa Institutional Animal Care and Use Committee guidelines.

Stereotaxic Microinfusion of Adeno-Associated Viruses into the LHA

Stereotaxic surgery was performed as previously described (15,17). Briefly, 6–7-week-old male mice were anesthetized with ketamine/xylazine (100:10 mg/kg i.p.) and placed on a stereotaxic apparatus (David Kopf Instruments, Tujunga, CA). Following standard disinfection, an ~1.0-cm incision was made to expose the skull, and a small hole was drilled into the skull bilaterally at defined positions (anteroposterior –1.5 mm; medial lateral +1.5 mm; dorsal ventral –4.9 mm with a 6° angle of injection arm), and a Hamilton microsyringe with small hub removable needle filled with adeno-associated virus (AAV) was slowly inserted. Injection was made by pressing the plunger at a rate of 0.05 μ L/min. After 10 min of waiting to ensure a full penetration of AAV into the targeted area, the needle was removed and the incision closed by wound clips. Mice were then kept on a warming pad until awake. At the end of the study, brains were extracted and postfixed in 4% paraformaldehyde, and the injection sites were confirmed for every case by observing the green fluorescence protein (GFP) signal blindly to physiological outcomes. Two of the 59 MC4R-TB mice receiving AAV-Cre-GFP were excluded from the final data analysis due to complete mistargeting of the LHA.

Quantification of Feeding Frequency and Locomotor Activity

Male mice aged 13–15 weeks were tested for locomotor activity using LABORAS (Metris, Hoofddorp, the Netherlands), an advanced system for automated recognition of small laboratory animal behaviors, such as locomotion, grooming, eating, and drinking. Data were collected uninterrupted in

the home cage over a 23-h period and then analyzed with LABORAS software as previously reported (18).

Energy Balance and Basal Blood/Plasma Analysis

After 1 week of full recovery from AAV microinfusion, mice were assigned ad libitum access to either a normal chow diet (#7913; Harlan Laboratories, Madison, WI) or a high-fat diet (HFD) (42% kcal from anhydrous milk fat, TD.88137; Harlan Laboratories). Body weight and food intake were measured periodically in both HFD and regular chow conditions up to 12 weeks after stereotaxic delivery of AAV into the LHA. For blood biochemistry, a trunk blood sample was collected from 18-week-old HFD-fed male mice. Sera were sent to the Vanderbilt University Mouse Metabolic Phenotyping Center for the measurement of blood hormone and cholesterol levels.

Glucose and Pyruvate Tolerance Tests

Seventeen- to 19-week-old male mice were used for glucose tolerance tests (GTTs) and pyruvate tolerance tests (PTTs). Mice were handled in the procedure room for 5 days before testing to allow habituation to the environment and to reduce handling stress. On the testing day, the mice were weighed, and food was removed at 9:00 A.M. for 6-h fasting with free access to water. At 3:00 P.M., blood glucose was measured at baseline (0') followed by immediate intraperitoneal injection of D-glucose (1 g/kg) (G8270; Sigma-Aldrich) or sodium pyruvate (2 g/kg) (P2256; Sigma-Aldrich). Blood glucose level was then monitored at 15, 30, 60, and 120 min for each mouse.

Intracerebroventricular Cannulation

Under continuous anesthesia, a small hole was drilled into the skull at a defined point (anteroposterior –0.2 mm, medial lateral +1.0 mm), and an intracerebroventricular (ICV) cannula with a specific length (0.23 mm below the plastic pedestal; Plastic One Inc.) was slowly inserted. The cannula was held in place with the appropriate amount of a glass ionomer luting cement anchored with a small machine screw in the right-front side of the cannula, allowing 3–5 min for stiffening. Open skin wounds were adhered onto mounted glass ionomer luting cement by applying Vetbond Tissue Adhesive, and the mice were kept on a warmed surgical table until fully awake.

Whole-Body Fluorodeoxyglucose Positron Emission Tomography/Computed Tomography Imaging

Whole-body fluorodeoxyglucose (FDG) scanning was performed in the Small Animal Imaging Core at the University of Iowa as previously reported (19). Seventeen- to 19-week-old, chow-fed male mice were used. Fasted animals (~14 h) were anesthetized with 1.5% isoflurane and their blood glucose measured before receiving a tail vein injection of FDG (7.5 ± 11.3 MBq). After a 60-min awake uptake period, the mice were imaged on an Inveon positron emission tomography (PET)/computed tomography (CT) scanner (Siemens, Knoxville, TN). A 15-min PET acquisition followed in the same workflow by a CT scan for attenuation correction

was acquired. Three days after the initial scan, the same animals underwent PET imaging again. The same imaging protocol was followed except 30 min before FDG injection, an intraperitoneal injection of melanotan II (MTII 2 mg/kg) (H-3902; Bachem) was given. All images were reconstructed using a three-dimensional OP-MAP algorithm. Image analysis was completed using PMOD version 3.2 (PMOD Technologies, Zurich, Switzerland). Volumes of interest were drawn for interscapular brown adipose tissue (iBAT), muscle, brain, kidney, and heart; organ-specific uptakes of FDG were calculated from the scanned images; and normalized change from baseline FDG uptake was compared between groups.

Direct Multifiber Recording of SNA

Regional SNA was measured by direct multifiber recording of sympathetic nerve branches subserving the iBAT and hindlimb muscles as previously described (20). Seventeen- to 19-week-old chow-fed male mice were used for SNA recording. Under anesthesia, catheterization of the carotid arteries and jugular vein was performed for hemodynamic recording and maintenance of anesthesia with α -chloralose (25 mg/kg/h), respectively. A nerve fascicle to iBAT or hindlimb was carefully isolated under a dissecting microscope. A bipolar platinum-iridium electrode (Cooner Wire) was suspended under the nerve and secured with silicone gel (Kwik-Cast, World Precision Instruments). The electrode was attached to a high-impedance probe (HIP-511; Grass Technologies), and the nerve signal was amplified 105 times with a Grass P5 AC preamplifier. After amplification, the nerve signal was filtered at a 100- and 1,000-Hz cutoff with a nerve traffic analysis system (model 706C; Department of Bioengineering, University of Iowa). Subsequently, the amplified and filtered nerve signal was routed to an oscilloscope (model 54501A; Hewlett-Packard) for monitoring the quality of the sympathetic nerve recording and to a resetting voltage integrator (model B600c; University of Iowa Bioengineering) that summed the total voltage output to a unit of $1 \text{ V} \times \text{s}/\text{min}$ before resetting to 0.

After a 10-min recording of baseline activity, mice received ICV infusion of MTII (2 μg). SNA was continuously monitored for 4 h, and change from baseline activity was calculated and compared between groups. At the end of study, mice received ICV infusion of 2 μL blue dye, and brains were extracted to confirm correct ICV cannulation and AAV injection site.

Bilateral iBAT Sympathetic Denervation

Bilateral iBAT sympathetic denervation was performed as previously reported (21), with slight modification. Thirteen- to 15-week-old chow-fed male mice were used for this study. On the day of surgery, each mouse was weighed and anesthetized with isoflurane. When the proper state of anesthesia was reached, the mouse was shaved of hair on the nape region and secured on a warm surgical table with a rectal probe to measure and maintain body temperature at 37.5°C. After a standard skin disinfection procedure, a lateral incision was made just below

the two shoulder blades to expose the intrascapular fat pads. A blunt forceps was then used to clamp the caudal edge of the intrascapular fat pad and retracted cranially over the head of the mouse. With this exposure, the bilateral sympathetic chain that innervates both the right- and the left-side BAT hemispheres was identified. All five branches of intercostal sympathetic nerves subserving the left- and right-side BAT fat pad were identified and carefully isolated, and the nerve branches between the root and the BAT were sectioned out (Fig. 4A–C). After completion of bilateral BAT denervation, the intrascapular fat pad was then returned to its original position and secured in place to the surrounding thoracic tissue and muscle with absorbable 6.0 VICRIL suture. A thin line of tissue adhesive (Vetbond) was applied along the edges of both skin flaps, and the two edges of skin were held in place until the entire length of the incision in the nape area was completely closed. Mice were monitored for 7 days postoperatively before subjected to further experimental procedures.

RNA Isolation and Real-Time PCR Analyses

Total RNA was isolated from snap-frozen iBAT and inguinal white adipose tissue (WAT) of 16–18-week-old chow-fed male mice, and cDNA was generated by reverse transcription as previously described (22). Quantitative real-time PCR was performed with SYBR green method using a standard protocol as previously described (22). The following primer sets were used to determine relative abundance and expression of UCP1, Cidea, PGC1a, β 3-AR, Glut1, and Glut4: 5'-AAGCTGTGCGATGTCCATGT-3' and 5'-AAGCCACAAACCCCTTTGAAAA-3' for UCP1, 5'-AGACAAATGTGCTTCCAAAAAGAA3' and 5'-GAAGAGATAAAGTTGTTGGTTTGGC-3' for PGC1a, 5'-GGTTC AAGGCCGTGTTAAGG-3' and 5'-CGTCATCTGTGCAGCATAGG-3' for Cidea, 5'-TCCTTCTACCTTCCCCTCCTT-3' and 5'-CGGCTTAGCCACAACGAACAC-3' for β 3-AR, 5'-CGCCCCCAGAAGGTTAT-3' and 5'-CGATGCGGTGGTCCAT-3' for Glut1, and 5'-TTGGCTCCCTTCAGTTTGG-3' and 5'-CTACCCAGCCACGTTGCAT-3' for Glut4. The expression of 36B4 (5'-CACTGGTCTAGGACCCGAGAAG-3' and 5'-GGTGCCCTGAAGATTTTCG-3') was used as an internal control gene.

Insulin Sensitivity and Western Blot Analysis

Nineteen- to 21-week-old overnight-fasted male mice were anesthetized with ketamine/xylazine (100:10 mg/kg) and received retro-orbital bolus insulin (5 units). iBAT, soleus muscle, and liver were then harvested at 10 min and snap frozen in liquid nitrogen. Small pieces of frozen tissue were homogenized in cold radioimmunoprecipitation assay buffer (#89901; Thermo Scientific) containing cocktails of proteinase inhibitors (11836170001; Roche Diagnostics) and phosphatase inhibitors (04906845001; Roche Diagnostics) and kept on ice for 30 min. Samples were then centrifuged (13,000 rpm) at 4°C for 20 min, and the supernatant was taken as total protein extraction. Protein concentration was determined by BCA protein assay method (#23228; Thermo Scientific), and 20 μg of protein

were separated by SDS-PAGE gel, transferred onto a polyvinylidene fluoride membrane, and immunoblotted with phosphorylation of v-akt murine thymoma viral oncogene homolog 1 (AKT) at Ser⁴⁷³ site (pAKT) (1/2,000) (#4060; Cell Signaling Technology), AKT (1/1,000) (#9272; Cell Signaling Technology), phosphorylation of extracellular-signal-regulated kinases (ERK) at Thr²⁰² and Tyr²⁰⁴ sites (pERK) (1/1,000) (#9101S; Cell Signaling Technology), and ERK (1/1,000) (#9102; Cell Signaling Technology) as previously reported (23). Membranes were then incubated with horseradish peroxidase-conjugated secondary antibody (Jackson ImmunoResearch), and signals were detected by chemiluminescence. Signal intensity was measured and analyzed by a BioSpectrum 810 Imaging System (UVP, Upland, CA). For each experiment, signal intensity of targeted proteins was normalized to total AKT or ERK signal intensity and then compared between groups.

Statistics

GraphPad Prism 5 software (GraphPad Software Inc., San Diego, CA) was used to perform all statistical analyses. Comparisons between groups were made by two-way or one-way ANOVA with Bonferroni post hoc analysis or by Student *t* test as indicated. *P* < 0.05 was considered statistically significant. Data are presented as mean ± SEM.

RESULTS

Restoration of MC4R^{LHA} Signaling Improves Impaired Glucose Tolerance in Obese MC4R-TB Mice Without Affecting Food Intake and Body Weight

To directly study the physiological function of MC4R^{LHA} signaling, we used AAV to specifically deliver Cre-recombinase-GFP (AAV-Cre-GFP) or GFP-alone (AAV-GFP) into the LHA of reactivatable MC4R-TB mice to remove a TB cassette and restore endogenous expression of MC4Rs. To optimize the delivery volume of AAV-Cre-GFP specifically into the LHA, we first performed microinfusion of AAV-Cre-GFP into the LHA of tdTomato reporter mouse in which a loxP-flanked TB cassette prevents transcription of a ubiquitous promoter-driven tdTomato, which can be re-expressed upon removal of the TB cassette by Cre-mediated recombination. Two weeks after AAV-Cre-GFP microinfusion, a large number of tdTomato⁺ and GFP⁺ cells were observed in the LHA, and nearly all of GFP⁺ cells were tdTomato⁺ (Fig. 1C), indicating that AAV-Cre-GFP properly induced Cre/loxP recombination in the LHA neurons with limited infection to the surrounding structures (Fig. 1B and C). The volume and titer of AAV-Cre-GFP were optimized by repeated injections in tdTomato reporter mice (data not shown). Using 0.3 μL/side at a titer of 1.18 × 10¹² genome copies/mL, we were able to achieve a maximum coverage of dorsomedial LHA, where MC4R-positive neurons are mainly located (Fig. 1A), with minimized infection of adjacent hypothalamic nuclei. After validation and optimization of the AAV microinfusion protocol, AAV-Cre-GFP or AAV-GFP was bilaterally infused into the LHA of MC4R-TB

mice and their wild-type (WT) littermates. In contrast to our hypothesis, restoration of MC4R^{LHA} expression had no measurable effects on body weight (Fig. 1D), food intake (Fig. 1E), locomotion (Fig. 1F), fasting glucose (Fig. 1G) and insulin (Fig. 1H) levels, body composition (Fig. 1L), or regional fat mass (Fig. 1M–O) when fed a chow diet. Subsequent assessment for glucose homeostasis, however, revealed that although both MC4R-TB groups were similarly obese (Fig. 1D), MC4R^{LHA} mice displayed significantly improved glucose tolerance compared with MC4R-TB (AAV-GFP) mice, especially at the 15' and 30' time points (Fig. 1I and J). To further test whether improved glucose tolerance is associated with altered insulin levels, we measured insulin levels at the 0', 15', and 30' time points after intraperitoneal injection of glucose (1 g/kg) and did not observe significant difference between the two MC4R-TB groups (Fig. 1K). Because none of these parameters was significantly different between the WT AAV-GFP (*n* = 5) and WT AAV-Cre-GFP (*n* = 5) groups, both groups of WT mice were combined and are referred to as control to increase statistical power.

Because MC4R-null mice are hypersensitive to a palatable HFD with marked hyperphagia and weight gain compared with the chow-fed condition (24,25), we generated another cohort of MC4R-TB mice by MC4R-TB homo × MC4R-TB het breeding paradigm and divided it into two groups to receive either AAV-GFP or AAV-Cre-GFP microinfusion. After 1 week of recovery from surgery, mice were fed an HFD to assess for a diet-specific effect of MC4R^{LHA} signaling. Restoration of MC4R^{LHA} signaling did not affect weight gain (Fig. 2A) or food intake (Fig. 2B) in the HFD condition. Although both groups of mice were similarly obese, fasting glucose level was significantly lower in MC4R^{LHA} mice (Fig. 2D) without a significant change in circulating insulin levels (Fig. 2C). A subsequent GTT again confirmed a significant improvement in glucose tolerance in MC4R^{LHA} mice (Fig. 1E and F). No differences were seen in fasting serum glucagon, leptin, free fatty acid, triglyceride, total cholesterol, or direct HDL levels (Fig. 2G–L). Collectively, these data demonstrate a role for MC4R^{LHA} signaling in the regulation of glucose tolerance without altering body energy balance or the levels of critical glucoregulatory hormones, such as insulin and glucagon.

MC4R^{LHA} Signaling Increases Glucose Uptake in iBAT Without Affecting Hepatic Gluconeogenesis or Insulin Sensitivity

Improved glucose tolerance in MC4R^{LHA} mice without a significant change in body weight or circulating insulin or glucagon levels led us to ask whether glucose disposal was increased in any tissue of MC4R^{LHA} mice. To this end, we performed whole-body PET/CT scanning for FDG uptake by which biodistribution of FDG can be quantified in a spatially resolved manner. Although both groups of MC4R-TB mice were similarly obese (Fig. 3B), FDG uptake was significantly increased in iBAT of MC4R^{LHA} mice (Fig. 3A and C) after MTII administration compared

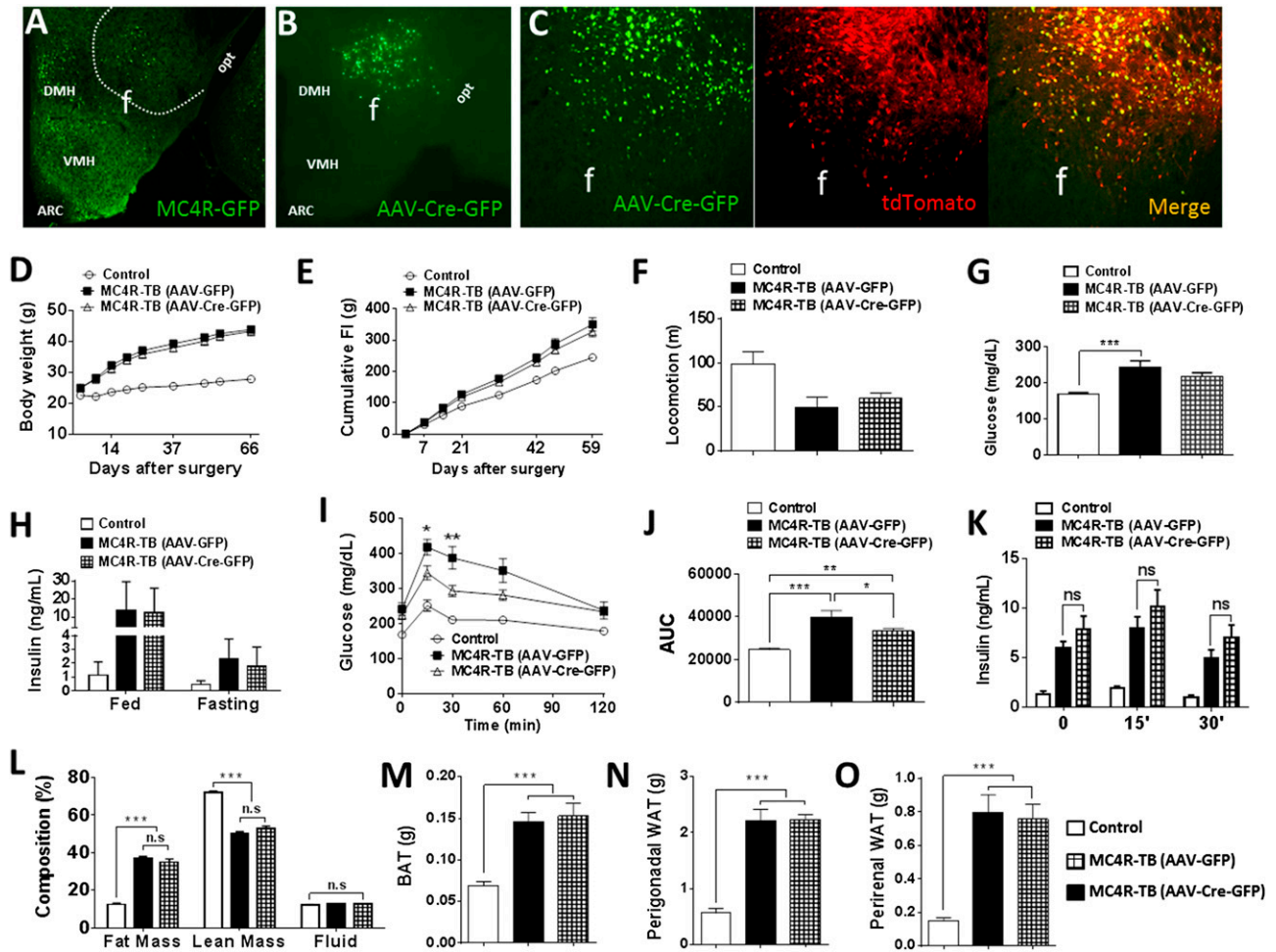


Figure 1—Reactivation of MC4R^{LHA} signaling improves glucose tolerance in chow-fed mice without affecting food intake and body weight. A–C: Representative images show the location of MC4R-GFP neurons in the dorsomedial part of LHA (A) where AAV-Cre-GFP microinfusion was made (B); AAV-Cre-GFP was validated in tdTomato reporter mouse by observing Cre-GFP (green) and tdTomato (red) fluorescent signals (C). After stereotaxic delivery of AAV into the LHA of young adult male mice, body weight gain (D), cumulative food intake (E), locomotor activity (F), basal blood glucose (G) and insulin (H) levels, GTT (I) and its AUC analysis (J), insulin secretion response to intraperitoneal glucose (1 g/kg) (K), body composition (L), and the mass of regional fat pads, including BAT (M), perigonadal WAT (N), and perirenal WAT (O), were measured in chow-fed mice. Data are mean ± SEM [for D–J and L–O, n = 10, 7, and 12 for control, MC4R-TB (AAV-GFP), and MC4R-TB (AAV-Cre-GFP), respectively; for K, n = 9, 7, and 8 for control, MC4R-TB (AAV-GFP), and MC4R-TB (AAV-Cre-GFP), respectively]. *P < 0.05, **P < 0.01, ***P < 0.001 by one-way or two-way ANOVA with Bonferroni post hoc analysis. ARC, arcuate nucleus of hypothalamus; AUC, area under the curve; DMH, dorsomedial hypothalamic nucleus; f, fornix; FI, food intake; opt, optic tract; VMH, ventromedial hypothalamic nucleus.

with control MC4R-TB (AAV-GFP) mice. A similar trend was noted in skeletal muscle but did not reach statistical significance (Fig. 3D). No difference in FDG uptake was found in brain (Fig. 3E), kidney, or heart (data not shown).

To further test whether MC4R^{LHA} signaling affects hepatic glucose production, a PTT was performed as an indirect measurement of hepatic gluconeogenesis. Intraperitoneal injection of sodium pyruvate (2 g/kg) in 6-h fasted animals sharply increased blood glucose levels within 15 min, which gradually returned to baseline levels by 2 h in control mice (Fig. 4B and C). In contrast, glucose levels continuously increased in both groups of MC4R-TB mice, and no significant difference was noted between the groups during the 2-h test (Fig. 4B and C), suggesting that

restoring MC4R^{LHA} signaling does not likely affect hepatic gluconeogenesis. Again, no difference of body weight was noted between the groups of MC4R-TB mice when performing GTT (Fig. 4A).

Additionally, to test the possibility that restoration of MC4R^{LHA} may affect insulin signaling, insulin-induced pAKT and ERK were also measured as markers of acute activation of the insulin receptor signaling cascade. After confirming a significant induction of pAKT and pERK by retro-orbital insulin bolus (5 units) in iBAT of WT mice (Fig. 4D and H), the same procedure was used to test insulin signaling in iBAT, soleus muscle, and liver. No significant difference was seen between the two MC4R-TB groups in any of the tissues tested (Fig. 4E–G and I–K), although there was a trend toward increased pERK/ERK

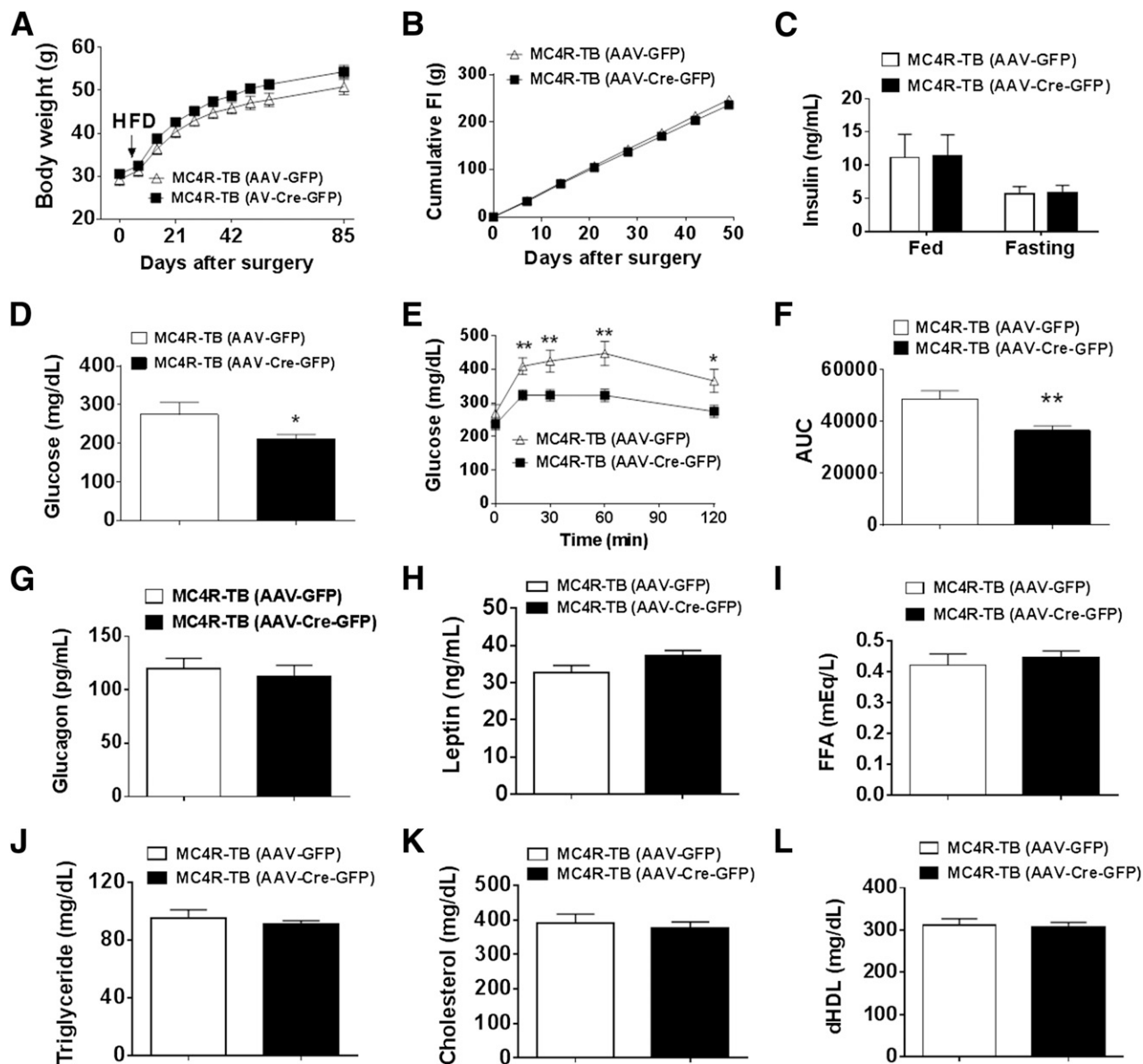


Figure 2—Reactivation of MC4R^{LHA} signaling improves hyperglycemia and glucose tolerance in HFD-fed mice without affecting food intake or body weight. After stereotaxic delivery of AAV into the LHA of young adult male MC4R-TB mice, body weight gain (A), cumulative food intake (B), basal blood insulin (C) and glucose (D) levels, GTT (E) and its AUC analysis (F), and blood glucagon (G), leptin (H), FFA (I), triglyceride (J), cholesterol (K), and dHDL (L) levels were measured in HFD-fed mice. Data are mean \pm SEM [$n = 9$ and 17 for MC4R-TB (AAV-GFP) and MC4R-TB (AAV-Cre-GFP), respectively]. * $P < 0.05$, ** $P < 0.01$ by two-way ANOVA with Bonferroni post hoc analysis or by Student t test. AUC, area under the curve; dHDL, direct HDL; FFA, free fatty acid; FI, food intake.

levels in soleus muscle that did not reach statistical difference (Fig. 4J).

Reactivation of MC4R^{LHA} Signaling Restores Blunted MTII-Induced iBAT Sympathetic Nerve Activation

The observation that MC4R^{LHA} mice display improved glucose tolerance and increased FDG uptake in iBAT without affecting circulating insulin or peripheral insulin sensitivity suggests the possibility that MC4R^{LHA} signaling may facilitate glucose uptake in iBAT by increasing SNA. Given the known role of the LHA in the regulation of sympathetic outflow and direct multisynaptic innervation

of LHA MC4R-positive neurons to iBAT (26,27), we tested the possibility that MC4R^{LHA} signaling mediates activation of SNA to iBAT induced by the melanocortin agonist MTII. Although direct multifiber recording demonstrated that control mice showed significantly increased iBAT SNA following infusion of MTII (Fig. 5A and B), the effect was completely abolished in MC4R-TB (AAV-GFP) mice (Fig. 5A and B). In contrast, MTII-induced iBAT SNA in MC4R^{LHA} mice was restored to control levels (Fig. 5A and B), indicating that reactivation of MC4R^{LHA} signaling is sufficient to rescue blunted sympathetic traffic to iBAT in obese MC4R-null mice. Because we noted a trend toward

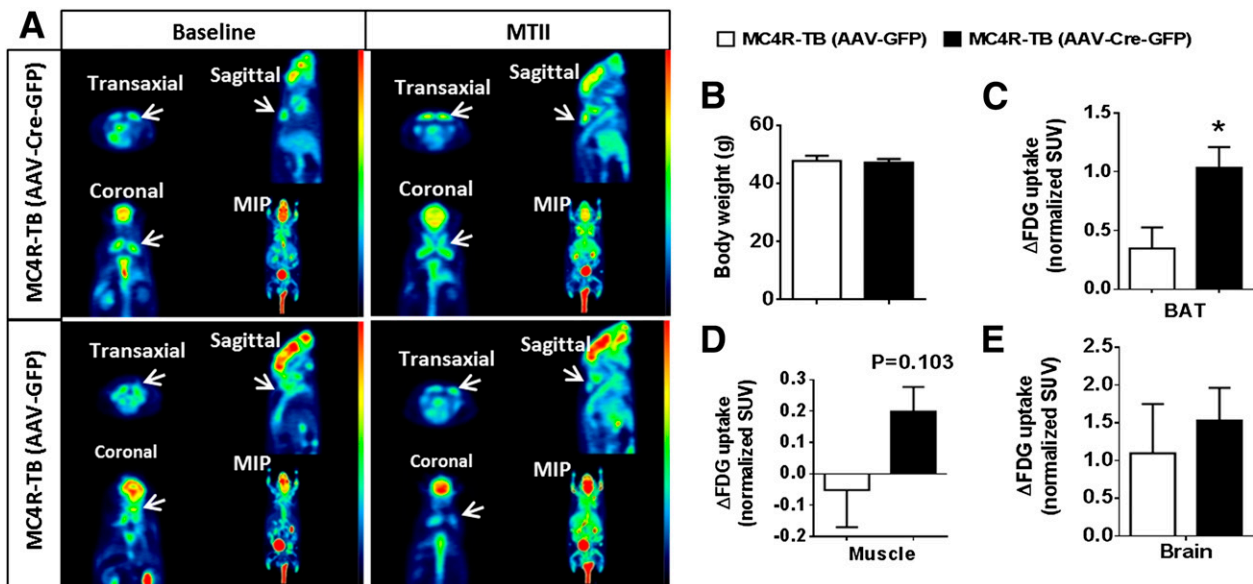


Figure 3—Restoration of MC4R^{LHA} signaling increases FDG uptake in iBAT. *A*: Representative images showing FDG uptake in iBAT at baseline and after MTII administration. *B*: Body weight of each group of mice used in FDG PET/CT scanning. *C–E*: The change of FDG uptake (normalized SUV) by MTII in iBAT (*C*), muscle (*D*), and brain (*E*). Data are mean ± SEM [$n = 6$ for both MC4R-TB (AAV-GFP) and MC4R-TB (AAV-Cre-GFP)]. * $P < 0.05$ by Student *t* test. MIP, maximum intensity projection; SUV, standardized uptake value.

increased FDG uptake in skeletal muscle, we also recorded lumbar nerve SNA to hindlimb skeletal muscle. As expected, the control group demonstrated a robust increase in lumbar SNA following ICV injection of MTII (Fig. 5C). MC4R-TB mice receiving AAV-GFP in the LHA displayed a significantly delayed and blunted response to MTII-induced lumbar SNA compared with WT mice, with a modest increase in lumbar SNA observed after 180 min of recording. This blunted response of MTII-induced lumbar SNA is restored to WT levels in MC4R^{LHA} mice (Fig. 5C). These results indicate that MC4R^{LHA} signaling mediates MTII-induced sympathetic activation to iBAT consistent with the increased glucose uptake observed in this tissue in MC4R^{LHA} mice. To further test whether altered iBAT SNA affects the body's thermoregulation, we measured core body temperature in a separate cohort of conscious mice by quick-inserting oiled rectal probe (Kent Scientific, Torrington, CT). In contrast to an earlier report (28), we found that obese MC4R-TB (AAV-GFP) mice have a slightly reduced core body temperature ($34.81 \pm 0.21^\circ\text{C}$) compared with WT control mice ($35.59 \pm 0.22^\circ\text{C}$), and a similar reduction was observed in MC4R-TB (AAV-Cre-GFP) mice ($34.80 \pm 0.23^\circ\text{C}$), suggesting that LHA MC4R signaling has no significant effect on core body temperature.

The Effect of MC4R^{LHA} Signaling on Gene Expression in iBAT and Inguinal WAT

Activation of mitochondrial energy dissipation pathways in iBAT has previously been linked with improved glucose tolerance (29). SNA is known to regulate the expression of genes involved in mitochondrial energy dissipation, including UCP1, Cidea, PGC1 α , β 3-AR, Glut1, and Glut4

(30). Therefore, we measured mRNA levels of these genes in iBAT to correlate changes of gene expression with SNA and FDG uptake. Gene expression profiling in iBAT revealed that significantly decreased expression of UCP1 and Cidea (Fig. 6A and B) but not PGC1 α and β 3-AR (Fig. 6C and D) in MC4R-TB mice was normalized in MC4R^{LHA} mice. Of note, although Glut1 expression was similarly increased in both MC4R-TB groups (Fig. 6E), a twofold increase in Glut4 expression was only observed in MC4R^{LHA} mice (Fig. 6F). None of these transcriptional changes were observed in inguinal WAT (Fig. 7A–F), indicating an iBAT-specific effect of SNA by MC4R^{LHA} signaling. Significantly increased expression of Glut4 in iBAT may at least partly explain the facilitated glucose uptake in iBAT and the ameliorated hyperglycemia observed after restoration of MC4R^{LHA} signaling.

iBAT Denervation Blocks Improved Glucose Tolerance in MC4R^{LHA} Mice

To directly demonstrate that SNA to iBAT is required for the improvement in glucose tolerance, another cohort of MC4R^{LHA} mice was generated and confirmed to have improved glucose tolerance without an effect on body weight (data not shown). One week after this GTT, mice underwent bilateral iBAT denervation by removal of five intercostal sympathetic nerve branches subserving iBAT (Fig. 8A–C) as previously described (21), which resulted in a significantly decreased UCP1 mRNA level compared with a sham control group in WT male mice, confirming effective iBAT denervation (Fig. 8D). One week after recovery from surgery, all three groups of mice were subjected to GTT again. Although there was no significant change in body

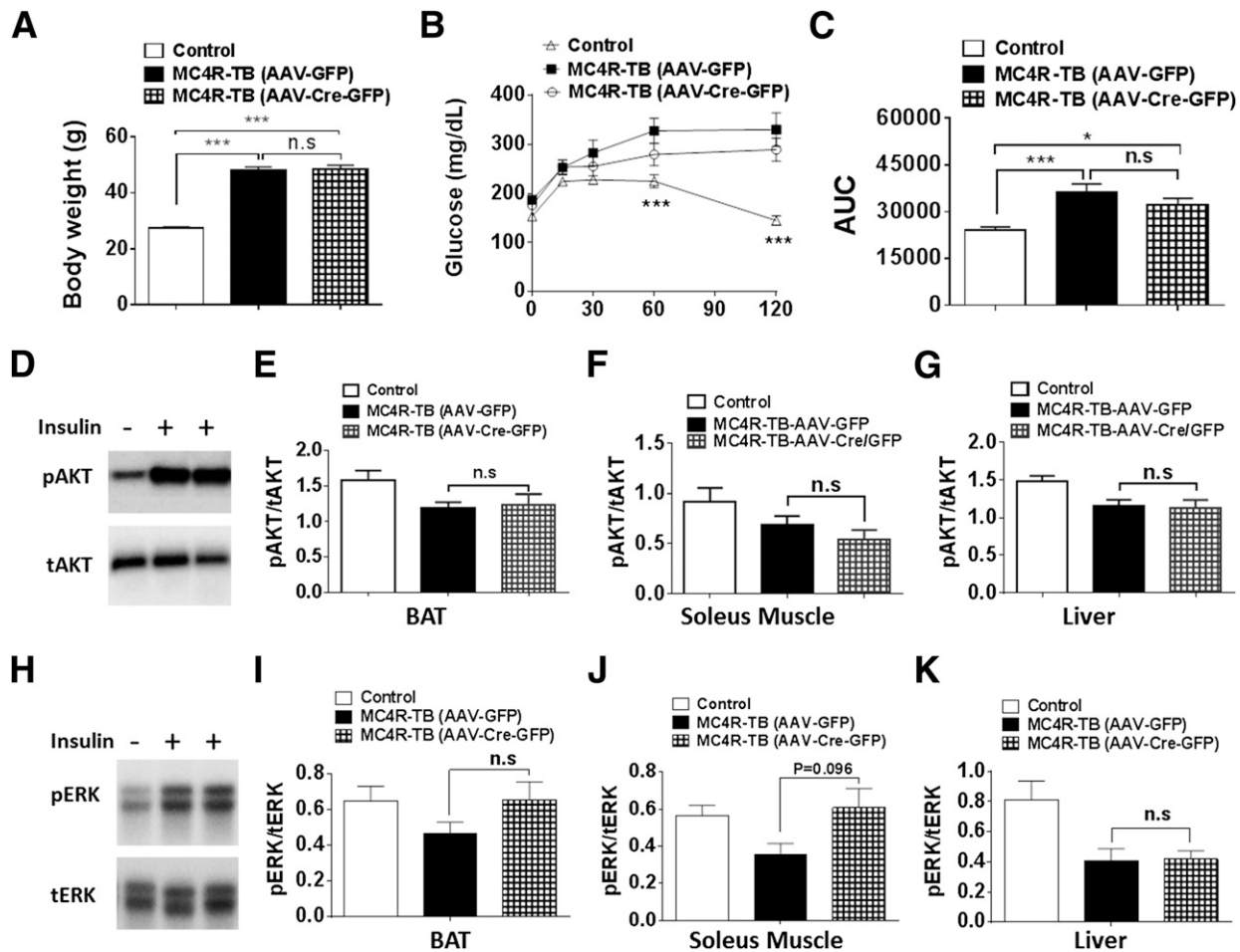


Figure 4—Restoration of MC4R^{LHA} signaling does not affect hepatic gluconeogenesis and peripheral insulin signaling. *A*: Body weight of each group of mice used in PTT. *B* and *C*: PTT (2 g/kg) and its AUC analysis [$n = 10, 9,$ and 11 for control, MC4R-TB (AAV-GFP), and MC4R-TB (AAV-Cre-GFP), respectively]. Representative Western blot image of bolus insulin (5 units)–mediated induction of pAKT (*D*) and pERK (*H*) in iBAT of WT mice. *E*–*G*: Immunoblotting quantification of an induction of pAKT by bolus insulin in iBAT (*E*), soleus muscle (*F*), and liver (*G*) ($n = 5$ – 6 /group). *I*–*K*: Immunoblotting quantification of an induction of pERK by bolus insulin in iBAT (*I*), soleus muscle (*J*), and liver (*K*) ($n = 7$ – 9 /group). Data are mean \pm SEM. * $P < 0.05$, *** $P < 0.001$ by one-way or two-way ANOVA with Bonferroni post hoc analysis. AUC, area under the curve; tAKT, total AKT; tERK, total ERK.

weight during the 1-week recovery period (Fig. 8E), the improved glucose tolerance seen in MC4R^{LHA} mice was lost following iBAT sympathetic denervation (Fig. 8F and G), confirming that iBAT SNA driven by MC4R^{LHA} signaling is required to improve glucose intolerance in obese MC4R-TB mice.

DISCUSSION

In the present study, we report a previously unappreciated role of MC4R^{LHA} signaling in the regulation of glucose metabolism through the regulation of sympathetic outflow to iBAT. This effect may be mediated in part by upregulated expression of Glut4 in iBAT. Of note, although genes that are known to promote energy dissipation during excess feeding, such as UCP1 and Cidea, were upregulated in iBAT of MC4R^{LHA} mice, no body weight effect was observed in either chow- or HFD-fed mice. This result is consistent, however, with a previous report that UCP1-deficient mice are cold sensitive but do not develop obesity under normal housing

conditions (31). The present findings suggest that the energy balance and glucoenergetic roles of iBAT can be dissociated. Consistent with this possibility, a thyroid hormone β -selective agonist and a β 3-AR agonist have been shown to increase SNA and thermogenesis in iBAT without increasing glucose uptake (32). These observations led us to speculate that MC4R^{LHA} signaling-mediated sympathetic outflow may differentially innervate a portion of iBAT that affects glucose utilization without altering energy expenditure or blunting the severe obesity seen in MC4R-null mice.

The primary effect we detected for MC4R^{LHA} signaling was on iBAT, and we also observed a potential role for skeletal muscle. A trend toward increased FDG uptake was noted in MC4R^{LHA} mice, and restoration of MC4R^{LHA} signaling showed a delayed response to MTII in lumbar SNA. Although these observed effects of MC4R^{LHA} signaling on muscle were less profound compared with iBAT, a potentially important contribution of muscle for the

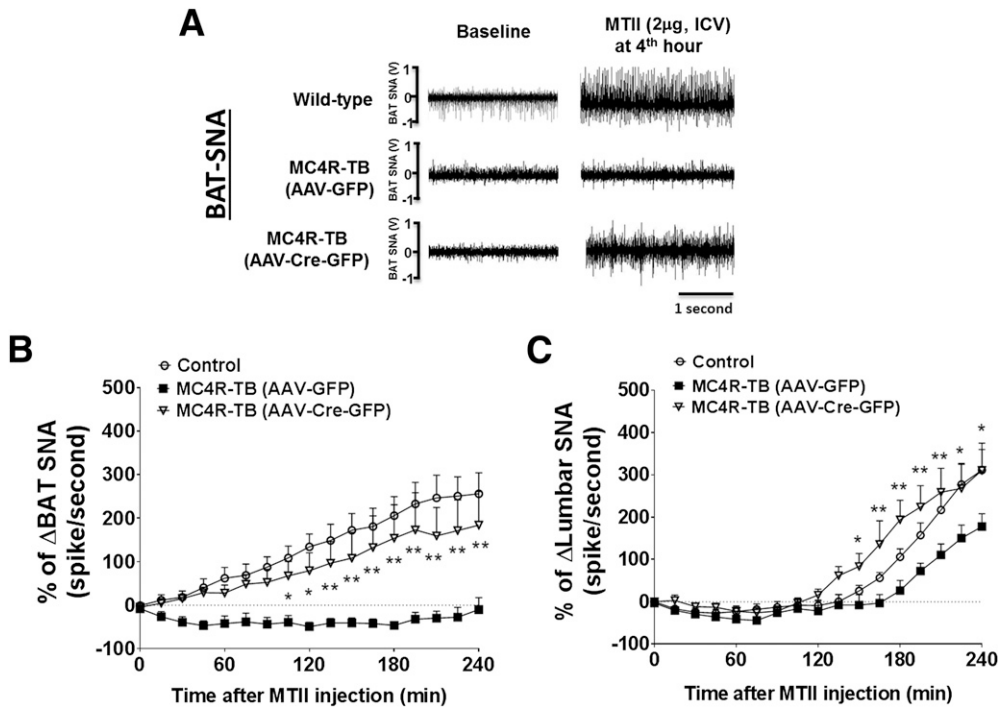


Figure 5—Reactivation of MC4R^{LHA} signaling normalizes impaired SNA response to MTII in iBAT and muscle of MC4R-null mice. *A*: Representative images showing iBAT SNA recording at baseline and at the 4th hour of ICV MTII. *B*: Four-hour time course of MTII-induced changes of iBAT SNA from baseline activity [*n* = 10, 7, and 7 for control, MC4R-TB (AAV-GFP), and MC4R-TB (AAV-Cre-GFP), respectively]. *C*: Four-hour time course of MTII-induced changes of lumbar SNA from baseline activity [*n* = 10, 6, and 6 for control, MC4R-TB (AAV-GFP), and MC4R-TB (AAV-Cre-GFP), respectively]. Data are mean ± SEM. **P* < 0.05, ***P* < 0.01 by two-way ANOVA with Bonferroni post hoc analysis [comparison between MC4R-TB (AAV-GFP) and MC4R-TB (AAV-Cre-GFP) groups].

glucoregulatory effect of MC4R^{LHA} signaling should be considered because there is a significantly larger volume of muscle compared with iBAT in humans. Another possibility

is that our ability to detect significant uptake of FDG by PET/CT imaging in muscle was limited by the challenging spatial resolution of a diffuse organ such as muscle. The mechanism of MTII-mediated increase in lumbar SNA is unclear. One possibility is that because MTII can also act on the melanocortin 3 receptor, which may account for the residual lumbar SNA response to MTII. Further work is needed to test this possibility.

Although we show that restoration of MC4R^{LHA} signaling does not affect circulating insulin levels as well as bolus insulin-activated signaling cascades in iBAT and liver, the role of insulin in the glucoregulatory effect of MC4R^{LHA} signaling should be considered because Glut4-mediated transport of glucose is insulin dependent (33) and there was a trend toward increased pERK activation in muscle. Additionally, it is important to note that most of these measures in the current study were performed in chow-fed mice, and insulin resistance in muscle of MC4R-null mice is markedly worse under HFD feeding conditions (34,35). A protective effect of MC4R^{LHA} activity on insulin signaling in muscle may only emerge under the severe insulin resistance that occurs during HFD feeding. Nevertheless, future work with hyperinsulinemic-euglycemic clamp in HFD fed mice may be needed to clarify the role of insulin in the glucoregulatory effect of MC4R^{LHA} signaling. Somewhat surprising to see was that restoration of MC4R^{LHA} signaling reduces glucose excursion

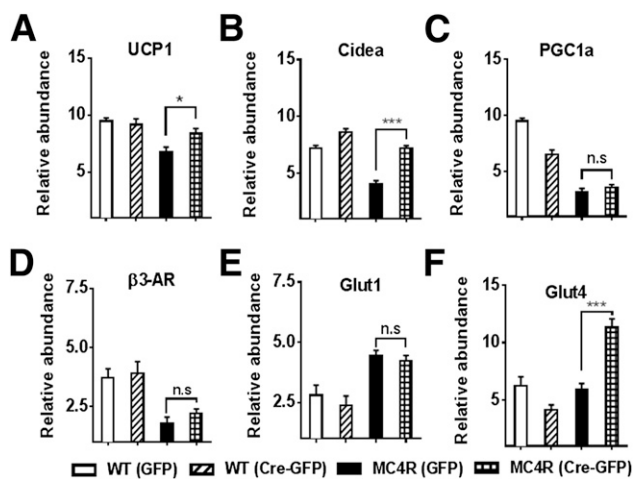


Figure 6—The effect of restoration of MC4R^{LHA} signaling on iBAT gene expression. Whole iBAT tissues were collected from chow-fed 16–18-week-old male mice (*n* = 6/group), snap frozen in liquid nitrogen, and processed for total mRNA extraction. Quantitative PCR was performed to determine relative abundance of expression of UCP1 (*A*), Cidea (*B*), PGC1a (*C*), β3-AR (*D*), Glut1 (*E*), and Glut4 (*F*). Data are mean ± SEM. **P* < 0.05, ****P* < 0.001 by one-way ANOVA with Bonferroni post hoc analysis.

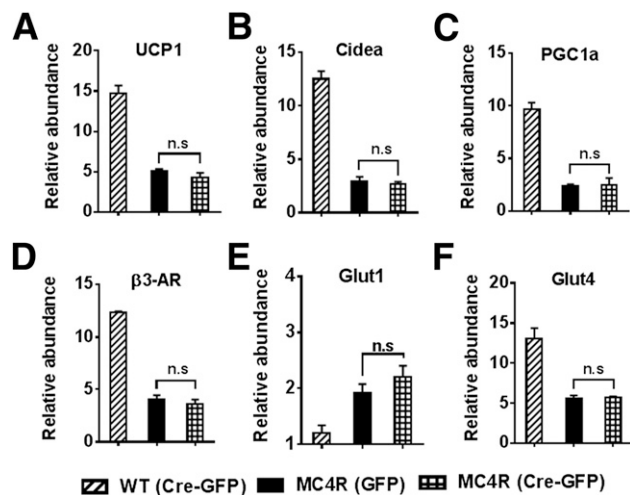


Figure 7—The effect of restoration of MC4R^{LHA} signaling on inguinal WAT gene expression. Whole iBAT tissues were collected from chow-fed 16–18-week-old male mice [*n* = 6 for each group of WT (AAV-Cre-GFP), MC4R-TB (AAV-GFP), and MC4R-TB (AAV-Cre-GFP) mice], snap frozen in liquid nitrogen, and processed for total mRNA extraction. Quantitative PCR was performed to determine relative abundance of expression of UCP1 (A), Cidea (B), PGC1a (C), β 3-AR (D), Glut1 (E), and Glut4 (F). Data are mean \pm SEM.

during GTT and fasting glucose levels in HFD-fed mice but without a concomitant reduction in insulin levels. In fact, there was a trend toward higher insulin levels during GTT in the MC4R^{LHA} group when the lower glycemic levels would predict lower insulin levels. This finding may indicate a degree of protection against obesity-related β -cell dysfunction conferred by MC4R^{LHA} activity. Whether such protection might be mediated by the demonstrated

improvement of glucose disposal in other tissues, by modulating factors such as GLP-1 or circulating nutrients (36), or by more direct action of MC4R^{LHA} activity on islets is unclear.

Although the current study uses a combination of Cre-lox technology and advanced physiological measures to assess the function of MC4R^{LHA} signaling, several limitations should be noted. We used the reactivation model in which MC4R expression is restored in the LHA of adult mice. This method is well suited to determine biological sufficiency but cannot determine whether redundancy in MC4R function exists. Indeed, a role for MC4R signaling in the regulation of autonomic activity has been reported for several other brain sites (37,38). Additionally, we attempted to control for off-target effects of Cre-recombinase expression by infusing both AAV-GFP and AAV-Cre-GFP WT groups. However, we cannot exclude the possibility that Cre expression affects FDG uptake because we did not include WT mice as controls due to cost. Many of the methods and assessments used here are technically challenging, labor intensive, and expensive, which limits the statistical power of certain assessments. Although the primary outcome measures are of large effect size, we cannot exclude the possibility that we were unable to discern subtle differences in secondary outcome measures. Finally, the relevance to human studies should be noted. Many studies have proposed increasing activity of BAT to treat metabolic disorders, such as obesity and diabetes (39). The current study is consistent with this approach, although it suggests that the effects of BAT activity on body weight and glucose tolerance may be dissociable, depending on the method used. However, any approach targeting

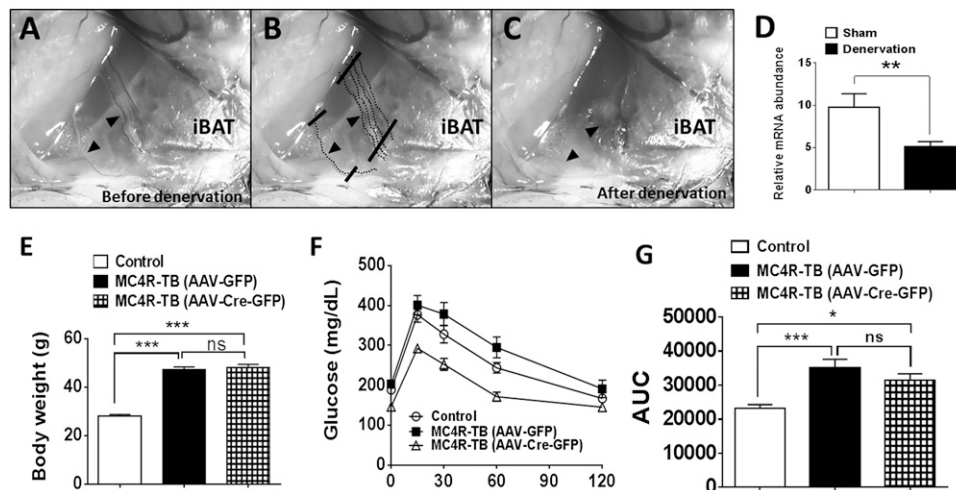


Figure 8—Bilateral iBAT denervation prevents the glucoregulatory effect of MC4R^{LHA} signaling. A: Representative image showing five branches of intercostal nerves (arrows) before denervation. B: Five branches of intercostal nerves were sectioned out as shown. C: Representative image showing postsurgical iBAT denervation. D: iBAT denervation in WT male mice significantly decreased UCP1 mRNA expression in iBAT compared with sham control WT mice. E: Body weight of each group of mice after 1 week of iBAT denervation. F and G: GTT and its AUC analysis after iBAT denervation. Data are mean \pm SEM. **P* < 0.05, ***P* < 0.01, ****P* < 0.001 by Student *t* test or one-way ANOVA with Bonferroni post hoc analysis. AUC, area under the curve.

SNA or BAT activity in humans may have limited therapeutic potential due to side effects. Even so, understanding the neural circuitry that improves glucose tolerance will be important to designing optimal treatments.

In summary, the results expand the understanding of how MC4R signaling differentially regulates a diverse set of physiological functions. Isolating the function of this neural circuit within the LHA also improves our understanding of how specific hypothalamic circuits control glucose tolerance. The results represent a novel mechanism by which brain MC4R signaling regulates glucose homeostasis independent of energy balance and may help in the development of novel strategies for the treatment of diabetes.

Acknowledgments. We thank Joel Elmquist (University of Texas Southwestern Medical Center, Dallas, TX) and Bradford Lowell (Beth Israel Deaconess Medical Center, Boston, MA) for use of the MC4R-TB mouse line.

Funding. This work was funded by the following grants: National Institutes of Health (R01-DK-097820 to A.W.N., MH-084058-01A1 to M.L., HL-084207 to K.R.), the University of Iowa Fraternal Order of Eagles Diabetes Center Pilot Grant to M.L., the American Heart Association (Established Investigator Award 14EIA18860041 to K.R., postdoctoral fellowship 12POST9120037 and Scientist Developmental grant 14SDG20140054 to H.C.), and the Brain & Behavior Research Foundation (formerly NARSAD) Young Investigator Award to H.C.

Duality of Interest. No potential conflicts of interest relevant to this article were reported.

Author Contributions. D.A.M. contributed to performing most critical experiments and to the data analysis and review and editing of the manuscript. L.N.M., T.Y., M.K., and J.J. contributed to the stereotaxic surgery, mouse breeding and genotyping, and Western blotting. M.R.A. and S.A.W. contributed to the PET/CT scanning for FDG uptake. L.L.B.P. contributed to the FDG uptake data analysis. A.W.N. contributed to the review and editing of the manuscript. M.L. and K.R. contributed to the experimental design and review and editing of the manuscript. H.C. contributed to the experimental design and to performing most critical experiments. H.C. is the guarantor of this work and, as such, had full access to all the data in the study and takes responsibility for the integrity of the data and the accuracy of the data analysis.

References

- Hossain P, Kavar B, El Nahas M. Obesity and diabetes in the developing world—a growing challenge. *N Engl J Med* 2007;356:213–215
- Myers MG Jr, Olson DP. Central nervous system control of metabolism. *Nature* 2012;491:357–363
- Kleinridders A, Könnner AC, Brüning JC. CNS-targets in control of energy and glucose homeostasis. *Curr Opin Pharmacol* 2009;9:794–804
- Cone RD. Anatomy and regulation of the central melanocortin system. *Nat Neurosci* 2005;8:571–578
- Vaisse C, Clement K, Durand E, Hercberg S, Guy-Grand B, Froguel P. Melanocortin-4 receptor mutations are a frequent and heterogeneous cause of morbid obesity. *J Clin Invest* 2000;106:253–262
- Huszar D, Lynch CA, Fairchild-Huntress V, et al. Targeted disruption of the melanocortin-4 receptor results in obesity in mice. *Cell* 1997;88:131–141
- Kishi T, Aschkenasi CJ, Lee CE, Mountjoy KG, Saper CB, Elmquist JK. Expression of melanocortin 4 receptor mRNA in the central nervous system of the rat. *J Comp Neurol* 2003;457:213–235
- Balthasar N, Dalggaard LT, Lee CE, et al. Divergence of melanocortin pathways in the control of food intake and energy expenditure. *Cell* 2005;123:493–505
- Cui H, Lutter M. The expression of MC4Rs in D1R neurons regulates food intake and locomotor sensitization to cocaine. *Genes Brain Behav* 2013;12:658–665
- Rossi J, Balthasar N, Olson D, et al. Melanocortin-4 receptors expressed by cholinergic neurons regulate energy balance and glucose homeostasis. *Cell Metab* 2011;13:195–204
- Xu Y, Elmquist JK, Fukuda M. Central nervous control of energy and glucose balance: focus on the central melanocortin system. *Ann N Y Acad Sci* 2011;1243:1–14
- Elias CF, Aschkenasi C, Lee C, et al. Leptin differentially regulates NPY and POMC neurons projecting to the lateral hypothalamic area. *Neuron* 1999;23:775–786
- Berthoud HR, Münzberg H. The lateral hypothalamus as integrator of metabolic and environmental needs: from electrical self-stimulation to optogenetics. *Physiol Behav* 2011;104:29–39
- Bernardis LL, Bellinger LL. The lateral hypothalamic area revisited: neuroanatomy, body weight regulation, neuroendocrinology and metabolism. *Neurosci Biobehav Rev* 1993;17:141–193
- Cui H, Sohn JW, Gautron L, et al. Neuroanatomy of melanocortin-4 receptor pathway in the lateral hypothalamic area. *J Comp Neurol* 2012;520:4168–4183
- Cui H, Mason BL, Lee C, Nishi A, Elmquist JK, Lutter M. Melanocortin 4 receptor signaling in dopamine 1 receptor neurons is required for procedural memory learning. *Physiol Behav* 2012;106:201–210
- Vialou V, Cui H, Perello M, et al. A role for Δ FosB in calorie restriction-induced metabolic changes. *Biol Psychiatry* 2011;70:204–207
- Xu P, Grueter BA, Britt JK, et al. Double deletion of melanocortin 4 receptors and SAPAP3 corrects compulsive behavior and obesity in mice. *Proc Natl Acad Sci U S A* 2013;110:10759–10764
- Duncan K, Rosean TR, Tompkins VS, et al. (18)F-FDG-PET/CT imaging in an IL-6- and MYC-driven mouse model of human multiple myeloma affords objective evaluation of plasma cell tumor progression and therapeutic response to the proteasome inhibitor ixazomib. *Blood Cancer J* 2013;3:e165
- Fernandes-Santos C, Zhang Z, Morgan DA, Guo DF, Russo AF, Rahmouni K. Amylin acts in the central nervous system to increase sympathetic nerve activity. *Endocrinology* 2013;154:2481–2488
- Pulinilkunnill T, He H, Kong D, et al. Adrenergic regulation of AMP-activated protein kinase in brown adipose tissue in vivo. *J Biol Chem* 2011;286:8798–8809
- Chuang JC, Cui H, Mason BL, et al. Chronic social defeat stress disrupts regulation of lipid synthesis. *J Lipid Res* 2010;51:1344–1353
- Brüning JC, Michael MD, Winnay JN, et al. A muscle-specific insulin receptor knockout exhibits features of the metabolic syndrome of NIDDM without altering glucose tolerance. *Mol Cell* 1998;2:559–569
- Butler AA, Marks DL, Fan W, Kuhn CM, Bartolome M, Cone RD. Melanocortin-4 receptor is required for acute homeostatic responses to increased dietary fat. *Nat Neurosci* 2001;4:605–611
- Srisai D, Gillum MP, Panaro BL, et al. Characterization of the hyperphagic response to dietary fat in the MC4R knockout mouse. *Endocrinology* 2011;152:890–902
- Voss-Andreae A, Murphy JG, Ellacott KL, et al. Role of the central melanocortin circuitry in adaptive thermogenesis of brown adipose tissue. *Endocrinology* 2007;148:1550–1560
- Song CK, Vaughan CH, Keen-Rhinehart E, Harris RB, Richard D, Barthess TJ. Melanocortin-4 receptor mRNA expressed in sympathetic outflow neurons to brown adipose tissue: neuroanatomical and functional evidence. *Am J Physiol Regul Integr Comp Physiol* 2008;295:R417–R428
- Ste Marie L, Miura GI, Marsh DJ, Yagaloff K, Palmiter RD. A metabolic defect promotes obesity in mice lacking melanocortin-4 receptors. *Proc Natl Acad Sci U S A* 2000;97:12339–12344
- Stanford KI, Middelbeek RJ, Townsend KL, et al. Brown adipose tissue regulates glucose homeostasis and insulin sensitivity. *J Clin Invest* 2013;123:215–223
- Harms M, Seale P. Brown and beige fat: development, function and therapeutic potential. *Nat Med* 2013;19:1252–1263
- Enerbäck S, Jacobsson A, Simpson EM, et al. Mice lacking mitochondrial uncoupling protein are cold-sensitive but not obese. *Nature* 1997;387:90–94

32. Matsen ME, Thaler JP, Wisse BE, et al. In uncontrolled diabetes, thyroid hormone and sympathetic activators induce thermogenesis without increasing glucose uptake in brown adipose tissue. *Am J Physiol Endocrinol Metab* 2013;304:E734–E746
33. Leto D, Saltiel AR. Regulation of glucose transport by insulin: traffic control of GLUT4. *Nat Rev Mol Cell Biol* 2012;13:383–396
34. Albarado DC, McClaine J, Stephens JM, et al. Impaired coordination of nutrient intake and substrate oxidation in melanocortin-4 receptor knockout mice. *Endocrinology* 2004;145:243–252
35. Sutton GM, Trevaskis JL, Hulver MW, et al. Diet-genotype interactions in the development of the obese, insulin-resistant phenotype of C57BL/6J mice lacking melanocortin-3 or -4 receptors. *Endocrinology* 2006;147:2183–2196
36. Komatsu M, Takei M, Ishii H, Sato Y. Glucose-stimulated insulin secretion: a newer perspective. *J Diabetes Investig* 2013;4:511–516
37. Sohn JW, Harris LE, Berglund ED, et al. Melanocortin 4 receptors reciprocally regulate sympathetic and parasympathetic preganglionic neurons. *Cell* 2013;152:612–619
38. Li P, Cui BP, Zhang LL, Sun HJ, Liu TY, Zhu GQ. Melanocortin 3/4 receptors in paraventricular nucleus modulate sympathetic outflow and blood pressure. *Exp Physiol* 2013;98:435–443
39. Chondronikola M, Volpi E, Børsheim E, et al. Brown adipose tissue improves whole-body glucose homeostasis and insulin sensitivity in humans. *Diabetes* 2014;63:4089–4099